Van Hove singularity induced phonon-mediated superconductivity above 77 K in hole-doped SrB_3C_3

Ting-Ting Gai,[1,*] Peng-Jie Guo,[2,3,*] Huan-Cheng Yang,[4,*] Yan Gao,[4] Miao Gao,[1,†] and Zhong-Yi Lu[4]

[1]*Department of Physics, School of Physical Science and Technology, Ningbo University, Zhejiang 315211, China*
[2]*Songshan Lake Materials Laboratory, Dongguan, Guangdong 523808, China*
[3]*Institute of Physics, Chinese Academy of Sciences, Beijing 100190, China*
[4]*Department of Physics, Renmin University of China, Beijing 100872, China*

(Received 12 February 2022; revised 9 May 2022; accepted 15 June 2022; published 27 June 2022)

To design a phonon-mediated superconductor with transition temperature above the liquid-nitrogen temperature under ambient pressure, we align the Fermi level of compound SrB_3C_3 to a Van Hove singularity by introducing 0.4 hole/f.u., namely $Rb_{0.4}Sr_{0.6}B_3C_3$. Based on density functional first-principles calculations and the Wannier interpolation technique, the electronic structure, lattice dynamics, and electron-phonon coupling (EPC) of $Rb_{0.4}Sr_{0.6}B_3C_3$ are investigated. Both the enlarged density of states at the Fermi level and the softened phonons play important roles to enhance the EPC. By solving the anisotropic Eliashberg equations, we find that the transition temperature of $Rb_{0.4}Sr_{0.6}B_3C_3$ is 83 K, successfully exceeding the liquid-nitrogen temperature at ambient pressure condition. Moreover, our calculations reveal that there is a single-gap to two-gap superconductivity transition in comparison with SrB_3C_3.

DOI: 10.1103/PhysRevB.105.224514

I. INTRODUCTION

According to the Bardeen-Cooper-Schrieffer theory [1], effective attractiveness between two electrons is mediated by lattice vibration, i.e., phonons, leading to the formation of Cooper pairs and superconductivity. Since too strong electron-phonon coupling (EPC) may result in lattice instability and trigger structural phase transition, how high the superconducting transition temperature (T_c) can reach for phonon-mediated superconductors remains confusing. The coupling between metallic σ-bonding bands and in-plane boron phonon modes in MgB_2 makes it a high-T_c superconductor with transition temperature being 39 K [2–7]. It was reported that the onset T_c of superconducting state in boron-doped Q-carbon is about 55 K, but the zero-resistivity condition was observed at 25 K [8]. In recent years, near-room-temperature hydrogen-rich superconductors were theoretically predicted and experimentally synthesized under ultrahigh pressure around 200 GPa, for example, H_3S, LaH_{10}, and YH_9 [9–15]. Obviously, such a high pressure significantly hinders the further application of hydrogen-rich high-T_c superconductors. To reduce the required pressure, several ternary compounds were proposed, including KB_2H_8 [16], $LaBH_8$ [17,18], and $LaBeH_8$ [19]. In particular, KB_2H_8 was suggested to superconduct at 134–146 K under a much lower pressure of 12 GPa. Very recently, cubic CeH_{10}, which is isostructural to LaH_{10}, was successfully synthesized, with T_c of 115 K at 95 GPa [20]. Despite these efforts, there still exists a huge gap in T_c for phonon-mediated superconductors at ambient and high pressure situations. For both scientific interest and practical application, finding a phonon-mediated superconductor above the liquid-nitrogen temperature at ambient pressure is extremely desired.

The T_c of phonon-mediated superconductors is influenced by three factors, namely the strength of EPC, characteristic phonon frequency, and density of states at the Fermi level $N(0)$. Under high pressure, the high T_c of hydrogen-rich superconductors markedly benefits from strong EPC and high-frequency hydrogen-related phonons [9–11,21]. At ambient pressure, the underlying physics of superconductivity in MgB_2 provides an unambiguous principle to acquire strong EPC through metallizing the σ-bonding bands. Guiding by this principle, several candidates of high-T_c conventional superconductor were proposed, exemplified by Li_xBC [22], boron-doped graphane [23], $Li_3B_4C_2$ [24], trilayer LiB_2C_2 film [25], and SrB_3C_3 [26]. These proposals indicate that a compound containing boron-carbon bonding network is an ideal platform to realize high-T_c superconductivity, whereas strong EPC and high-frequency phonon conditions can be satisfied simultaneously. In particular, SrB_3C_3 has already been synthesized in experiment at around 50 GPa [27], and it remains dynamically stable under ambient pressure according to the calculated phonon spectrum [26,27]. It was predicted that SrB_3C_3 is a single-gap anisotropic s-wave superconductor, with EPC constant λ and T_c being 0.92 and 40 K [26], comparable to those of MgB_2. To further boost T_c, the last factor that can be utilized is enlarging $N(0)$; in other words, aligning the Fermi level to approach a Van Hove singularity by doping. It is noted that the Van Hove singularity should be in the vicinity of the Fermi level, because heavy electron/hole doping will induce lattice instability.

As shown by density functional theory (DFT) calculations, the Fermi level of SrB_3C_3 locates in a narrow valley of the density of states (DOS). There are two Van Hove singularities

*These three authors contributed equally to this work.
†gaomiao@nbu.edu.cn

in the DOS just below and above the Fermi level [26], resulting from two flat bands along the $X - M$ direction in the Brillouin zone. Since reducing the occupation of σ-bonding bands is beneficial to superconductivity, the Fermi level can be shifted downwards to exactly match one of these two Van Hove singularities to induce high-T_c superconductivity. Accordingly, 0.4 holes/f.u. should be introduced. In particular, it was recently predicted that the sp^3-bonded boron-carbon structure of SrB_3C_3 can remain in $Rb_xSr_{1-x}B_3C_3$ for x being 0.5 [28]. Thus it is quite interesting to know whether phonon-mediated superconductivity can be realized above the liquid-nitrogen temperature at ambient pressure in compound $Rb_{0.4}Sr_{0.6}B_3C_3$ by pinning the Fermi level to a Van Hove singularity. In this work, we report the electronic structure, lattice dynamics, EPC, and phonon-mediated superconductivity in compound $Rb_{0.4}Sr_{0.6}B_3C_3$, based on the DFT calculations in combination with the Wannier interpolation. We find that $N(0)$ is improved to 1.72 times that of SrB_3C_3. The EPC constant λ in $Rb_{0.4}Sr_{0.6}B_3C_3$ is accurately determined to be 1.49, which can give rise to superconductivity with T_c of 83 K by solving the anisotropic Eliashberg equations.

II. METHODS

In our calculations, the first-principles package, QUANTUM-ESPRESSO, was adopted [29]. We calculated the electronic states and phonon perturbation potentials [30] using the generalized gradient approximation (GGA) of the Perdew-Burke-Ernzerhoff formula for the exchange and correlation functional [31] and the optimized norm-conserving Vanderbilt pseudopotentials [32]. The hole doping is dealt with virtual crystal approximation (VCA). After a convergence test, the kinetic energy cutoff and the charge density cutoff were chosen to be 80 Ry and 320 Ry, respectively. The charge densities were calculated on an unshifted **k** mesh of $16 \times 16 \times 16$ points in combination with a Methfessel-Paxton smearing [33] of 0.02 Ry. The dynamical matrices and the perturbation potentials were computed on a Γ-centered $4 \times 4 \times 4$ mesh, within the framework of density-functional perturbation theory [34]. To construct the maximally localized Wannier functions (MLWFs) [35], we chose 24 sp^3-hybridized states localized in the middle of boron-carbon bonds and $4p$ orbitals of rubidium or strontium. The convergent EPC constant λ was extensively carried out through fine electron ($60 \times 60 \times 60$) and phonon ($20 \times 20 \times 20$) grids with electron-phonon Wannier (EPW) codes [36]. The Dirac δ functions for electrons and phonons were smeared out by a Gaussian function with the widths of 50 meV and 0.5 meV, respectively. A fine electron grid of $40 \times 40 \times 40$ points was employed when solving the anisotropic Eliashberg equations. The sum over Matsubara frequencies was truncated with $\omega_c = 1.0$ eV, about ten times that of the highest phonon frequency.

III. RESULTS AND DISCUSSIONS

The space group of SrB_3C_3 is $Pm\bar{3}n$, whereas strontium, boron, and carbon occupy the $2a$(0.0, 0.0, 0.0), $6c$(0.25, 0.0, 0.5), and $6d$(0.25, 0.5, 0.0) Wyckoff positions, respectively. Since Rb doping is treated with VCA, the inner atomic coordinates are unchanged. Compared with

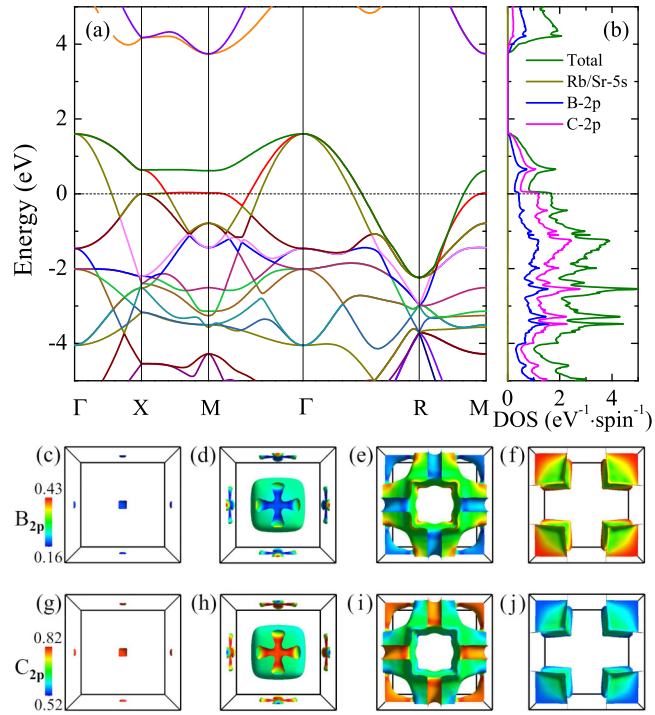

FIG. 1. Electronic structure for $Rb_{0.4}Sr_{0.6}B_3C_3$. (a) Band structure. The Fermi level is set to zero. (b) Total and orbital-resolved density of states. Distributions of B-$2p$ orbitals (c)–(f) and C-$2p$ orbitals (g)–(j) on the Fermi surfaces.

4.8776 Å in SrB_3C_3 [26], the lattice constant of $Rb_{0.4}Sr_{0.6}B_3C_3$ slightly increases to 4.9056 Å. Figure 1 shows the electronic structure of $Rb_{0.4}Sr_{0.6}B_3C_3$. Compared with the one of SrB_3C_3, the Fermi level is shifted downwards by 0.35 eV [Fig. 1(a)], corresponding to a Van Hove singularity in the DOS [Fig. 1(b)]. As a consequence, the $N(0)$ is enlarged to 1.69 states/spin/eV/cell, about 1.72 times that of SrB_3C_3. In addition, the DOS is dominated by the B-$2p$ and C-$2p$ orbitals, especially the C-$2p$ orbitals, which contribute 70.4% to $N(0)$ [Fig. 1(b)]. There are four partially occupied energy bands, leading to complicated Fermi surfaces [Figs. 1(c)–1(f)]. The weights of B-$2p$ and C-$2p$ orbitals in the Kohn-Sham states on the Fermi level are color mapped. Specifically, a pocket around the X point [Fig. 1(h)], a cross centered at the X point [Fig. 1(i)], and triangular Fermi surfaces near the M point [Fig. 1(j)] are dominated by the C-$2p$ orbitals. For the multichannel tubelike Fermi surface, the B-$2p$ orbitals have certain proportion at the corners [Fig. 1(e)]. The distribution of B-$2p$ orbitals mainly locate on the cubic Fermi surface surrounding the R point [Fig. 1(f)]. Interestingly, there is a tilted Dirac point on the $X - M$ line at the Fermi level.

Figure 2 shows the phonon spectrum, phonon DOS $F(\omega)$, Eliashberg spectral function $\alpha^2F(\omega)$, and accumulated $\lambda(\omega)$ for $Rb_{0.4}Sr_{0.6}B_3C_3$. The dynamical stability of $Rb_{0.4}Sr_{0.6}B_3C_3$ is confirmed by the phonon spectrum, whereas no imaginary phonon frequency is found [Fig. 2(a)]. This means that $Rb_{0.4}Sr_{0.6}B_3C_3$ can exist at ambient pressure as a metastable structure. In comparison with SrB_3C_3, the low-frequency gap

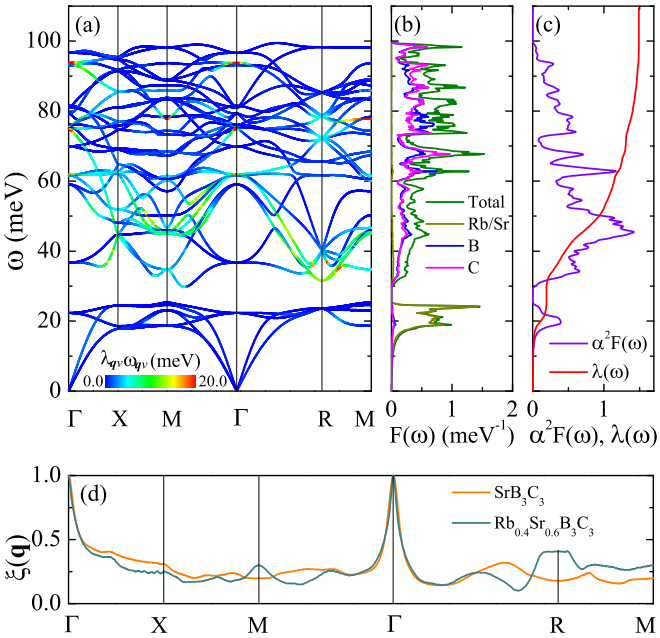

FIG. 2. Lattice dynamics of $Rb_{0.4}Sr_{0.6}B_3C_3$. (a) Phonon spectrum, with a color representation of $\lambda_{\mathbf{q}\nu}\omega_{\mathbf{q}\nu}$. (b) Phonon DOS $F(\omega)$. (c) Eliashberg spectral function $\alpha^2F(\omega)$ and accumulated $\lambda(\omega)$. The accumulated $\lambda(\omega)$ is computed using the formula $2\int_0^\omega \frac{1}{\omega'}\alpha^2F(\omega')d\omega'$. (d) Comparison of Fermi surfaces nesting between $Rb_{0.4}Sr_{0.6}B_3C_3$ and SrB_3C_3. $\xi(\mathbf{q})$ equals $\sum_{nm\mathbf{k}}\delta(\epsilon^n_{\mathbf{k}})\delta(\epsilon^m_{\mathbf{k}+\mathbf{q}})/N_{\mathbf{k}}$. Here, n and m are the indices of energy bands. $\epsilon^n_{\mathbf{k}}$ and $\epsilon^m_{\mathbf{k}+\mathbf{q}}$ represent the eigenvalues of the electronic states with respect to the Fermi energy. $N_{\mathbf{k}}$ stands for the total number of $\mathbf{k}$ points in the fine mesh. $\xi(\mathbf{q})$ is normalized by $\xi(\mathbf{\Gamma})$.

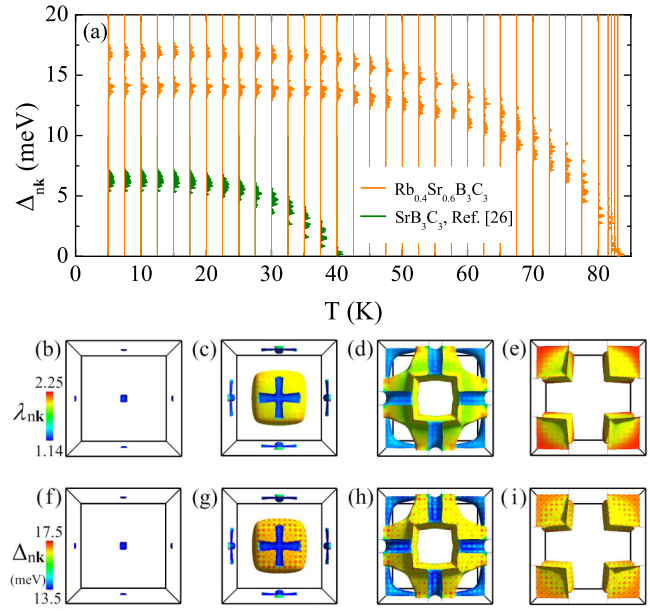

FIG. 3. (a) Normalized superconducting gap distribution of $Rb_{0.4}Sr_{0.6}B_3C_3$ at different temperatures. In comparison, the temperature-dependent distribution of superconducting gap in SrB_3C_3 was given. (b)–(e) The momentum-resolved EPC strength $\lambda_{n\mathbf{k}}$ for each electronic state $n\mathbf{k}$ on the Fermi surface. (f)–(i) Distribution of superconducting gap $\Delta_{n\mathbf{k}}$ on the Fermi surface at 5 K.

slightly increases to 5.16 meV. Below the gap, the phonon modes mainly involve the vibrations of Rb/Sr atoms, as shown by the atom-projected phonon DOS [Fig. 2(b)]. For the entire frequency range, the boron and carbon atoms have equal contribution to the phonon DOS. There exist several strongly coupled phonon modes from 30 meV to 70 meV [Fig. 2(a)], corresponding to a broadening peak in the Eliashberg spectral function $\alpha^2F(\omega)$ [Fig. 2(c)]. Consequently, the accumulated $\lambda(\omega)$ caused by the broadening $\alpha^2F(\omega)$ peak occupies 74.5% of total λ. For SrB_3C_3, the highest peak of $\alpha^2F(\omega)$ locates around 73 meV [26]. In addition to $N(0)$, the redshifted peak of $\alpha^2F(\omega)$ in $Rb_{0.4}Sr_{0.6}B_3C_3$ indicates that the phonon softening plays a notable role to enhance the EPC, particularly near the R point. In general, the softening can be driven by nesting between segments of the surface Fermi contours. Here, we calculate the Fermi surface nesting function to elucidate whether it can account for the softened phonons around the R point in $Rb_{0.4}Sr_{0.6}B_3C_3$ [Fig. 2(d)]. The nesting function near the R point exhibits dramatic aggrandizement with respect to other $\mathbf{q}$ points in the Brillouin zone. Thus we can conclude that the phonon softening around the R point is caused by the Fermi surfaces nesting. Owning the accurate $\alpha^2F(\omega)$, we find that the EPC constant λ is 1.49, which is more than twice that of SrB_3C_3. The logarithmic average frequency is calculated to be 44.37 meV, almost unchanged with respect to the case before doping. Utilizing the McMillan-Allen-Dynes formula, the T_c of $Rb_{0.4}Sr_{0.6}B_3C_3$ is estimated to be 58.3 K, by setting the screened Coulomb potential μ^* to 0.1.

It has been demonstrated that the predicted T_c is more reasonable by solving the anisotropic Eliashberg equations, when the anisotropy of the Fermi surface is strong [7,16,25,26,36]. For example, the McMillan-Allen-Dynes T_c of SrB_3C_3 is 32.9 K. It increases to 40 K if taking the anisotropic distribution of momentum-resolved EPC strength $\lambda_{n\mathbf{k}}$ on the Fermi surface into consideration [26]. Figure 3(a) shows the normalized superconducting gap distribution of $Rb_{0.4}Sr_{0.6}B_3C_3$ at different temperatures. Interestingly, there is a single-gap to two-gap superconductivity transition from SrB_3C_3 to $Rb_{0.4}Sr_{0.6}B_3C_3$. At 5 K, these two average superconducting gaps $\Delta_{n\mathbf{k}}$ are 16.78 meV and 13.92 meV, respectively. It was recently suggested that $Rb_{0.333}Sr_{0.667}B_3C_3$ and $Rb_{0.5}Sr_{0.5}B_3C_3$ can superconduct at about 63–78 K by setting the screened Coulomb potential μ^* to 0.1–0.13 [28]. If we adopt the same value of μ^*, the T_c of $Rb_{0.4}Sr_{0.6}B_3C_3$ is determined to be 79–83 K. Therefore, $Rb_{0.4}Sr_{0.6}B_3C_3$ is a promising phonon-mediated superconductor with T_c above the liquid-nitrogen temperature at ambient pressure. The distribution of $\lambda_{n\mathbf{k}}$ on the Fermi surface resembles that of B-2p orbitals [Figs. 3(b)–3(e)]. This unambiguously suggests that the B-2p orbitals have strong coupling with phonons. While, the coupling between C-2p orbitals and phonons is relatively weak. The superconducting gaps $\Delta_{n\mathbf{k}}$ distribute similarly with $\lambda_{n\mathbf{k}}$ [Figs. 3(f)–3(i)]. Consequently, the physical origin for two-gap superconductivity in $Rb_{0.4}Sr_{0.6}B_3C_3$ comes from the fact that the phonons have different coupling strengths with the B-2p and C-2p orbitals.

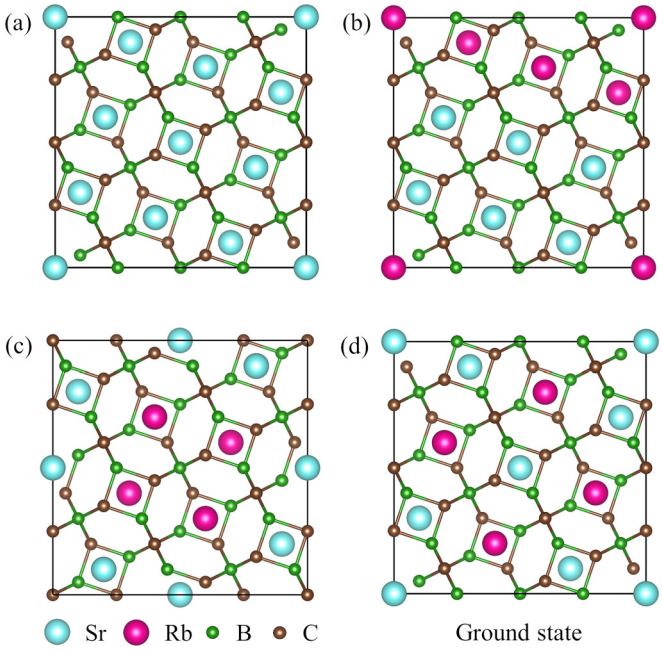

FIG. 4. (a) Top view of the $\sqrt{5} \times \sqrt{5} \times 1$ supercell for SrB_3C_3. (b) Line-type distribution of Rb atoms for $Rb_{0.4}Sr_{0.6}B_3C_3$. (c) Cluster-type distribution of Rb atoms for $Rb_{0.4}Sr_{0.6}B_3C_3$. (d) The ground-state structure for $Rb_{0.4}Sr_{0.6}B_3C_3$ in the $\sqrt{5} \times \sqrt{5} \times 1$ supercell.

Physically, VCA is a good treatment for the partial replacement of Sr with Rb, since they are the nearest neighbors in the Periodic Table. Here, we also examine the influence of VCA on the above results. According to the structure prediction based on cluster expansion and the CALYPSO code, the clathrate geometry of boron and carbon is unchanged upon hole doping for $Rb_xSr_{1-x}B_3C_3$, with x changing from 0.125 to 0.5 [28]. This indicates that the total energy of $Rb_xSr_{1-x}B_3C_3$ is dominated by the distribution of introduced Rb atoms for given doping concentration x. In order to find the ground-state structure of $Rb_{0.4}Sr_{0.6}B_3C_3$, we calculate the total energies for several kinds of distribution of Rb atoms in $\sqrt{5} \times \sqrt{5} \times 1$ supercell (Fig. 4), whereas there are four Rb and six Sr atoms. In particular, the Rb atoms in the structure presented in Fig. 4(d) are as evenly distributed as possible. By setting the total energy of this structure to zero, we find that the line-type and cluster-type structures are energetically unfavorable, with energy disadvantages being 164.7 meV/cell and 150.0 meV/cell, respectively. This means that the Rb atoms tend to form an even-distributed pattern as shown in Fig. 4(d).

Although, the direct computation of EPC of the $\sqrt{5} \times \sqrt{5} \times 1$ supercell is quite difficult, we can evaluate the impact of VCA by comparing the electron and phonon DOS between VCA and supercell calculations. As shown in Fig. 5(a), the DOS curves obtained by these two methods almost completely merge together from -1.6 eV to 1.6 eV. Most importantly, the Fermi level still locates on the Van Hove singularity, as shown by the DOS of the supercell. This strongly suggests that the results of VCA well approximate the electronic structure of the supercell. The phonon DOS also

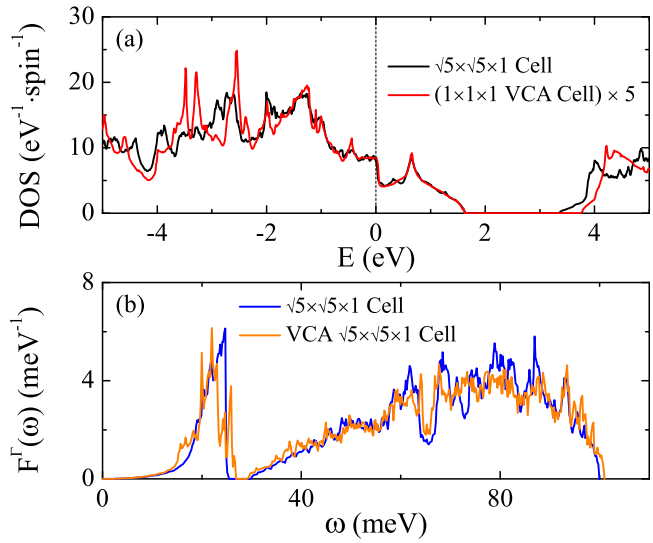

FIG. 5. (a) Electron DOS comparison between VCA cell and $\sqrt{5} \times \sqrt{5} \times 1$ supercell for $Rb_{0.4}Sr_{0.6}B_3C_3$. (b) Phonon DOS comparison. In order to gain a clear view, the VCA phonon DOS is also computed in $\sqrt{5} \times \sqrt{5} \times 1$ cell, whereas Rb and Sr atoms are replaced with a virtual one containing 40% Rb and 60% Sr. The phonon DOS $F^{\Gamma}(\omega)$ is obtained by the following procedure. First, we calculate the dynamical matrix at the Γ point. And then, the real-space force constants are generated by the inverse Fourier transformation of the Γ-point dynamical matrix. At last, through generalized Fourier transformation, we can compute the phonon frequencies of arbitrary **q** points in dense grid, which are employed to construct the DOS.

exhibits good consistency, especially between 30 meV and 70 meV [Fig. 5(b)]. Since the phonons in this frequency region have strong coupling with electrons [Fig. 2(a)], thus we can conclude that the VCA treatment has minor influence on EPC and phonon-mediated superconductivity of $Rb_{0.4}Sr_{0.6}B_3C_3$.

We calculate the formation enthalpy of $Rb_{0.4}Sr_{0.6}B_3C_3$ to study its thermodynamic stability under pressure (Fig. 6). As a comparison, the formation enthalpies of rubidium, strontium, boron, carbon, SrB_6, SrB_3C_3, and $RbSrB_6C_6$ are also

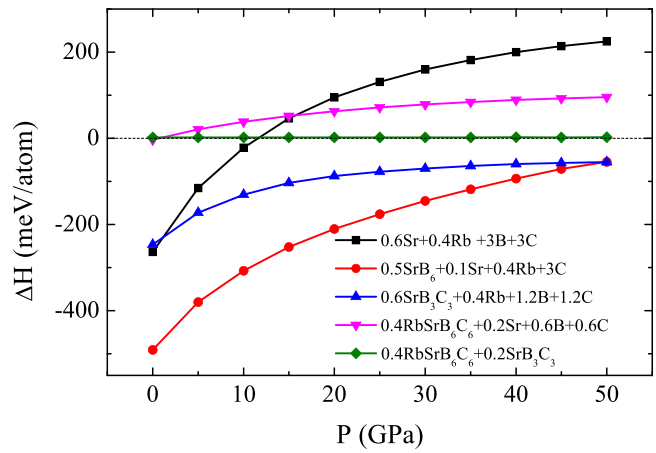

FIG. 6. Formation enthalpy comparison between $Rb_{0.4}Sr_{0.6}B_3C_3$ and selected reaction paths under different pressure. For clarity, the formation enthalpy of $Rb_{0.4}Sr_{0.6}B_3C_3$ at each pressure is set to zero.

computed, respectively. The sequences of pressure-driven phase transitions for elemental solids of rubidium, strontium, and boron are as follows. For rubidium, the transition from body-centered cubic (bcc) structure to face-centered cubic (fcc) phase occurs at 7.0 GPa [37]. The crystal structure of Rb-III is orthorhombic with space group $C222_1$, which is stable between 13 and 17 GPa [38]. Rb-IV is an incommensurate host-guest composite structure, which transforms to a body-centered tetragonal $I4_1/amd$ structure (Rb-V) at 19.6 GPa [39,40] and then to a face-centered orthorhombic *Cmca* structure (Rb-VI) at 48.5 GPa [41]. It was suggested that *Cmca* is the most stable structure up to 143 GPa [42]. fcc structure is the ground state of strontium under ambient pressure. It transforms to bcc structure at 3.5 GPa [43]. Although, it was found experimentally that strontium undergoes several intermediate phases under 50 GPa, namely $I4_1/amd$ Sr-III [44], monoclinic Sr-IV [45], and incommensurate Sr-V [46]. Surprisingly, theoretical calculation revealed that the bcc structure will transform to a *Cmcm* phase at 25 GPa, which is more favorable at least to 50 GPa, compared with the structural models proposed in experiment [47]. Thus the *Cmcm* phase is employed in our calculation. For boron, phase transformations take place at 19 GPa from $\alpha - B_{12}$ to $\gamma - B_{28}$ and 89 GPa from $\gamma - B_{28}$ to α-Ga-type structure [48]. For carbon, the diamond structure is used for the entire pressure range shown in Fig. 6. For compound SrB_6, the ambient $Pm\bar{3}m$ structure transforms to an orthorhombic *Cmmm* structure at 48 GPa and then to a tetragonal $I4/mmm$ structure at 60 GPa [49]. Although $Rb_{0.4}Sr_{0.6}B_3C_3$ is metastable versus the combination of SrB_6/SrB_3C_3 and corresponding solids, it dominates the constituent elemental solids above 10 GPa. Moreover, the stability of $Rb_{0.4}Sr_{0.6}B_3C_3$ overwhelms $0.4RbSrB_6C_6 + 0.2Sr + 0.6B + 0.6C$ from 5 GPa. Interestingly, the formation enthalpy of $Rb_{0.4}Sr_{0.6}B_3C_3$ is always slightly lower in comparison with that of $0.4RbSrB_6C_6 + 0.2SrB_3C_3$.

According to the electronic structure of SrB_3C_3 [26,27], there are two Van Hove singularities in the vicinity of the Fermi level. We further investigate the EPC and phonon-mediated superconductivity in 0.25 electrons/f.u. doped SrB_3C_3, namely $Sr_{0.75}La_{0.25}B_3C_3$, whereas the Fermi level is pinned to the upper Van Hove singularity. It is found that $N(0)$ and λ are equal to 1.58 states/spin/eV/cell and 1.13. Compared with $Rb_{0.4}Sr_{0.6}B_3C_3$, these two quantities are reduced by 8.1%, and 24.2%, respectively. As a consequence, the T_c is determined to be 59 K, by solving the anisotropic Eliashberg equations and setting μ^* to 0.1.

IV. CONCLUSION

In summary, we have proposed a feasible strategy to realize phonon-mediated superconductivity above the liquid-nitrogen temperature under ambient pressure by adjusting the Fermi level of SrB_3C_3 to match a Van Hove singularity, forming $Rb_{0.4}Sr_{0.6}B_3C_3$. By means of the first-principles calculations and the Wannier interpolation, we have presented the results of electronic structure, lattice vibrations, EPC, and superconductivity of $Rb_{0.4}Sr_{0.6}B_3C_3$. The EPC in $Rb_{0.4}Sr_{0.6}B_3C_3$ is significantly enhanced with respect to that in SrB_3C_3, due to the synergic effects of softened phonon modes and enlarged DOS at the Fermi level. The T_c of $Rb_{0.4}Sr_{0.6}B_3C_3$ is determined to be 77.5–83 K by the solution of anisotropic Elishberg equations. Furthermore, it is revealed that $Rb_{0.4}Sr_{0.6}B_3C_3$ is a two-gap superconductor. This can be rationalized in terms of the different coupling strengths with B-2p and C-2p orbitals for phonons. The influence of VCA is also discussed in detail.

ACKNOWLEDGMENTS

This work was supported by the National Natural Science Foundation of China (Grants No. 11974194 and No. 11934020) and the China Postdoctoral Science Foundation (Grant No. 2020TQ0347). M.G. was sponsored by K. C. Wong Magna Fund in Ningbo University.

[1] J. Bardeen, L. N. Cooper, and J. R. Schrieffer, Phys. Rev. **108**, 1175 (1957).
[2] J. Nagamatsu, N. Nakagawa, T. Muranaka, Y. Zenitani, and J. Akimitsu, Nature (London) **410**, 63 (2001).
[3] J. M. An and W. E. Pickett, Phys. Rev. Lett. **86**, 4366 (2001).
[4] Y. Kong, O. V. Dolgov, O. Jepsen, and O. K. Andersen, Phys. Rev. B **64**, 020501(R) (2001).
[5] T. Yildirim, O. Gülseren, J. W. Lynn, C. M. Brown, T. J. Udovic, Q. Huang, N. Rogado, K. A. Regan, M. A. Hayward, J. S. Slusky, T. He, M. K. Haas, P. Khalifah, K. Inumaru, and R. J. Cava, Phys. Rev. Lett. **87**, 037001 (2001).
[6] H. J. Choi, D. Roundy, H. Sun, M. L. Cohen, and S. G. Louie, Phys. Rev. B **66**, 020513(R) (2002).
[7] H. J. Choi, D. Roundy, H. Sun, M. L. Cohen, and S. G. Louie, Nature (London) **418**, 758 (2002).
[8] A. Bhaumik, R. Sachan, S. Gupta, and J. Narayan, ACS Nano **11**, 11915 (2017).
[9] D. Duan, Y. Liu, F. Tian, D. Li, X. Huang, Z. Zhao, H. Yu, B. Liu, W. Tian, and T. Cui, Sci. Rep. **4**, 6968 (2014).
[10] H. Liu, I. I. Naumov, R. Hoffmann, N. W. Ashcroft, and R. J. Hemley, Proc. Natl. Acad. Sci. USA **114**, 6990 (2017).
[11] F. Peng, Y. Sun, C. J. Pickard, R. J. Needs, Q. Wu, and Y. Ma, Phys. Rev. Lett. **119**, 107001 (2017).
[12] A. P. Drozdov, M. I. Eremets, I. A. Troyan, V. Ksenofontov, and S. I. Shylin, Nature (London) **525**, 73 (2015).
[13] A. P. Drozdov, P. P. Kong, V. S. Minkov, S. P. Besedin, M. A. Kuzovnikov, S. Mozaffari, L. Balicas, F. F. Balakirev, D. E. Graf, V. B. Prakapenka, E. Greenberg, D. A. Knyazev, M. Tkacz, and M. I. Eremets, Nature (London) **569**, 528 (2019).
[14] M. Somayazulu, M. Ahart, A. K. Mishra, Z. M. Geballe, M. Baldini, Y. Meng, V. V. Struzhkin, and R. J. Hemley, Phys. Rev. Lett. **122**, 027001 (2019).
[15] E. Snider, N. Dasenbrock-Gammon, R. McBride, X. Wang, N. Meyers, K. V. Lawler, E. Zurek, A. Salamat, and R. P. Dias, Phys. Rev. Lett. **126**, 117003 (2021).

[16] M. Gao, X.-W. Yan, Z.-Y. Lu, and T. Xiang, Phys. Rev. B **104**, L100504 (2021).
[17] S. Di Cataldo, C. Heil, W. von der Linden, and L. Boeri, Phys. Rev. B **104**, L020511 (2021).
[18] X. Liang, A. Bergara, X. Wei, X. Song, L. Wang, R. Sun, H. Liu, R. J. Hemley, L. Wang, G. Gao, and Y. Tian, Phys. Rev. B **104**, 134501 (2021).
[19] Z. Zhang, T. Cui, M. J. Hutcheon, A. M. Shipley, H. Song, M. Du, V. Z. Kresin, D. Duan, C. J. Pickard, and Y. Yao, Phys. Rev. Lett. **128**, 047001 (2022).
[20] W. Chen, D. V. Semenok, X. Huang, H. Shu, X. Li, D. Duan, T. Cui, and A. R. Oganov, Phys. Rev. Lett. **127**, 117001 (2021).
[21] N. Bernstein, C. S. Hellberg, M. D. Johannes, I. I. Mazin, and M. J. Mehl, Phys. Rev. B **91**, 060511(R) (2015).
[22] H. Rosner, A. Kitaigorodsky, and W. E. Pickett, Phys. Rev. Lett. **88**, 127001 (2002).
[23] G. Savini, A. C. Ferrari, and F. Giustino, Phys. Rev. Lett. **105**, 037002 (2010).
[24] M. Gao, Z.-Y. Lu, and T. Xiang, Phys. Rev. B **91**, 045132 (2015).
[25] M. Gao, X.-W. Yan, Z.-Y. Lu, and T. Xiang, Phys. Rev. B **101**, 094501 (2020).
[26] J.-N. Wang, X.-W. Yan, and M. Gao, Phys. Rev. B **103**, 144515 (2021).
[27] L. Zhu, G. M. Borstad, H. Liu, P. A. Guńka, M. Guerette, J.-A. Dolyniuk, Y. Meng, E. Greenberg, V. B. Prakapenka, B. L. Chaloux, A. Epshteyn, R. E. Cohen, and T. A. Strobel, Sci. Adv. **6**, eaay8361 (2020).
[28] P. Zhang, X. Li, X. Yang, H. Wang, Y. Yao, and H. Liu, Phys. Rev. B **105**, 094503 (2022).
[29] P. Giannozzi, S. Baroni, N. Bonini, M. Calandra, R. Car, C. Cavazzoni, D. Ceresoli, G. L. Chiarotti, M. Cococcioni, I. Dabo *et al.*, J. Phys.: Condens. Matter **21**, 395502 (2009).
[30] F. Giustino, M. L. Cohen, and S. G. Louie, Phys. Rev. B **76**, 165108 (2007).
[31] J. P. Perdew, K. Burke, and M. Ernzerhof, Phys. Rev. Lett. **77**, 3865 (1996).
[32] D. R. Hamann, Phys. Rev. B **88**, 085117 (2013).
[33] M. Methfessel and A. T. Paxton, Phys. Rev. B **40**, 3616 (1989).
[34] S. Baroni, S. de Gironcoli, A. Dal Corso, and P. Giannozzi, Rev. Mod. Phys. **73**, 515 (2001).
[35] G. Pizzi, V. Vitale, R. Arita, S. Blügel, F. Freimuth, G. Granton, M. Gibertini, D. Gresch, C. Johnson, T. Koretsune *et al.*, J. Phys.: Condens. Matter **32**, 165902 (2020).
[36] S. Poncé, E. R. Margine, C. Verdi, and F. Giustino, Comput. Phys. Commun. **209**, 116 (2016).
[37] D. A. Young, *Phase Diagrams of the Elements* (University of California Press, Berkeley, CA, 1991).
[38] R. J. Nelmes, M. I. McMahon, J. S. Loveday, and S. Rekhi, Phys. Rev. Lett. **88**, 155503 (2002).
[39] H. Olijnyk and W. B. Holzapfel, Phys. Lett. A **99**, 381 (1983).
[40] M. I. McMahon, S. Rekhi, and R. J. Nelmes, Phys. Rev. Lett. **87**, 055501 (2001).
[41] U. Schwarz, K. Syassen, A. Grzechnik, and M. Hanfland, Solid State Commun. **112**, 319 (1999).
[42] Y. Ma, A. R. Oganov, and Y. Xie, Phys. Rev. B **78**, 014102 (2008).
[43] H. Olijnyk and W. B. Holzapfel, Phys. Lett. A **100**, 191 (1984).
[44] D. R. Allan, R. J. Nelmes, M. I. McMahon, S. A. Belmonte, and T. Bovornratanaraks, Rev. High Press. Sci. Technol. **7**, 236 (1998).
[45] T. Bovornratanaraks, D. R. Allan, S. A. Belmonte, M. I. McMahon, and R. J. Nelmes, Phys. Rev. B **73**, 144112 (2006).
[46] M. I. McMahon, T. Bovornratanaraks, D. R. Allan, S. A. Belmonte, and R. J. Nelmes, Phys. Rev. B **61**, 3135 (2000).
[47] D. Young Kim, P. Srepusharawoot, C. J. Pickard, R. J. Needs, T. Bovornratanaraks, R. Ahuja, and U. Pinsook, Appl. Phys. Lett. **101**, 052604 (2012).
[48] A. R. Oganov, J. Chen, C. Gatti, Y. Ma, Y. Ma, C. W. Glass, Z. Liu, T. Yu, O. O. Kurakevych, and V. L. Solozhenko, Nature (London) **457**, 863 (2009).
[49] L. Zhu, G. M. Borstad, R. E. Cohen, and T. A. Strobel, Phys. Rev. B **100**, 214102 (2019).